Cellular Communication Network Factor 3 contributes to the pathological process of rheumatoid arthritis through promoting cell senescence and osteoclastogenesis in the joint

Running title: Role of CCN3 in development of RA

Authors

Taiki Tokuhiro[1], Gen Matsumae[1], Tsutomu Endo[1], Yuki Ogawa[1], Takuya Ogawa[1], Liyile Chen[1], Yoshio Nishida[1], Hend Alhasan[1], Hideyuki Kobayashi[1], Taku Ebata[1], Tomohiro Shimizu[1], Daisuke Takahashi[1], Tomohiro Onodera[1], Ken Kadoya[1], M Alaa Terkawi[1*], Norimasa Iwasaki[1],

[1]Department of Orthopedic Surgery, Faculty of Medicine and Graduate School of Medicine, Hokkaido University, Kita-15, Nish-7, Kita-ku, Sapporo, 060-8638, Japan.

***Corresponding Author**: M Alaa Terkawi, DVM, PhD, Department of Orthopaedic Surgery, Faculty of Medicine and Graduate School of Medicine, Hokkaido University, Kita-15, Nishi-7, Kita-ku, Sapporo, Japan.

Telephone: +81-11-706-5935, Fax: +81-11-706-6054.

E-mail: materkawi@med.hokudai.ac.jp

Abstract

Rheumatoid arthritis (RA) is a chronic systemic and autoimmune disease that primarily affects joints and causes pain, stiffness and swelling. The affected joints exhibit severe inflammation in the synovium and bone erosion, leading to joint deformity. Aging is an important factor facilitating the development of RA, as it is associated with an increase in the number of senescent cells, autoantibodies and proinflammatory cytokines in tissues. Given that CCN3 is highly expressed in RA joints and that its level is associated with the severity of the disease, we explored its molecular function in joints and therapeutic potential in RA. An analysis of public scRNA-seq data from the RA synovium revealed that CCN3 is expressed by an inflammatory fibroblast subset. Interestingly, stimulation with CCN3 resulted in the activation of the senescence pathway in synoviocytes and osteoclast differentiation in monocytes in vitro. Consistent with these results, the administration of CCN3 into the knee joint and onto the calvarial bone resulted in increased numbers of senescent synoviocytes in the joint and osteoclasts in the bone, respectively. Furthermore, the therapeutic potential of targeting CCN3 was evaluated in an experimental RA model. Administration of the CCN3 antibody significantly suppressed inflammation and osteoclast numbers in the joints of the RA model mice. Our findings suggest that CCN3 contributes to pathological processes in RA and represents a promising therapeutic target for the treatment of RA.

Key words: Rheumatoid arthritis, Senescence, Osteoclastogenesis, CCN3

1. INTRODUCTION

Rheumatoid arthritis (RA) is a systemic autoimmune disease that manifests predominantly as progressive synovial inflammation and cartilage/bone destruction in one or more joints. The health consequences of disease include the disability of patients, who lose their ability to perform regular life functions [1]. The disease is highly prevalent; in 2019, 18 million people were estimated to be affected by RA worldwide, 70% of whom were women older than 55 years. The epidemiology of the disease will continue to increase as life expectancy increases. The progression of RA involves three stages: (1) the preclinical phase, which comprises the onset of autoimmune disorders at the cellular level; (2) the clinical phase, which comprises the induction of strong inflammatory responses and the onset of clinical symptoms; and (3) the extra-articular manifestation phase, which comprises destruction of the joint [6].

Therapeutic options include medications for the management of symptoms, physical therapy for reducing joint stress and surgical intervention for reducing pain and restoring joint function [2]. Emerging evidence underlines that the use of immunomodulatory agents such as TNF blockade for the treatment of RA is often not effective in elderly individuals due to factors such as immunosenescence, increased infection risk, and comorbidities [3][4][5]. Therefore, continuing research on RA is essential for the development of new effective therapeutic agents.

Aging is the fundamental factor involved in the development of autoimmune disorders, as elderly people exhibit immune cell dysfunction accompanied by increases in

autoantibodies and proinflammatory cytokines. Recent evidence has demonstrated that the onset of RA is typified by the accumulation of senescent cells in synovial tissue, namely macrophages and synoviocytes, which are the key effector cells in the pathogenesis of RA [7][8][9]. In response to internal or external stimuli and stress, cells activate the p53-cyclin-dependent kinase inhibitor 1A (Cdkn1a; p21) and/or retinoblastoma (RB)-Cdkn2a (p16) pathways, resulting in G1/S cell cycle blockade. The senescent cells can initiate tissue dysfunction due to the loss of their homeostatic functions and the development of a senescence-associated secretory phenotype (SASP) in cells that secrete high levels of proinflammatory and extracellular matrix degradation mediators [10]. Therefore, the blockade of senescence would be an alternative approach for the treatment of RA, which has fewer side effects than immunosuppressive agents do [10]. This requires a better understanding of the senescence mechanism in synovium and identification of the factors that activate this process in vivo.

In this context, Communication network factor 3 (CCN3), also known as nephroblastoma overexpressed (NOV), is a matricellular protein of the CCN family that has been shown to play an important role in aging-associated diseases, such as osteoarthritis, coronary artery disease, obesity, insulin resistance, cancer and chronic inflammation [11][12][13][14][15][16]. Many studies have demonstrated that CCN3 levels in the serum of patients are associated with the severity of RA [17][18][19]. Therefore, we hypothesized that CCN3 might act as factor involving in activation of senescence in the joint, and directed our study on elucidating the role of CCN3 in the progression of RA. Our data revealed that CCN3

acts as an autocrine/paracrine factor involved in the activation of cellular senescence and osteoclastogenesis and thus represents a promising target for the treatment of RA.

2. MATERIALS AND METHODS

2.1. Ethics statement

The protocols for the use of human samples in our experiments were approved by the Research Ethics Review Board of Hokkaido University Hospital with the consent of patients/donors (Approval Nos. 020-0078; 21-0044). Animal experiments were conducted with the approval of the Hokkaido University Graduate School of Medicine Animal Experiment Facility Committee (20-0065).

2.2. Immunohistochemistry (IHC) staining of synovial tissues

Synovial tissue was collected from rheumatoid arthritis patients who underwent total knee or wrist arthroplasty. Control tissue was collected from osteoarthritis patients who underwent total knee arthroplasty. Synovial tissues were fixed with formalin, embedded in paraffin, and then sectioned into slices (3 μm thick) for immunohistochemical staining, which was performed with a CCN3 antibody (Novus Biologicals, USA). The signals were amplified with a horseradish peroxidase–conjugated specific antibody, followed by counterstaining with hematoxylin (Wako, Japan).

2.3. In vitro *stimulation assays with recombinant CCN3*

Human fibroblast-like synoviocytes (hFLSs), purchased from Cell Applications (San Diego, CA), were cultured in α-modification minimum essential medium (αMEM)

supplemented with 10% heat-inactivated fetal bovine serum, 1% penicillin/streptomycin, and 1% l-glutamine (growth medium) at 37°C in a humidified 5% CO2 atmosphere and stimulated with CCN3 (100 ng/mL) for 24 h, 48 h or 168 h. Cultures were replenished with fresh medium every 3 days. Thereafter, the cells were subjected to gene and protein expression analyses. On the other hand, human monocytes were isolated from healthy blood donors via density gradient centrifugation (Ficoll-PaqueTM PLUS: GE Healthcare) and then isolated via a MACS Pan monocyte isolation kit (Miltenyi Biotec, Auburn). Monocytes were cultured for 6 days in growth medium supplemented with 25 ng/mL human recombinant macrophage colony-stimulating factor (hMCSF; Peprotech, Cranbury, NJ) and then stimulated with 100 ng/mL CCN3 (R&D Systems) for 24 h. For the osteoclast assay, monocytes were cultured in growth medium supplemented with 25 ng/mL hMCSF (Peprotech) to produce osteoclast precursors. The cells were then cultured in the same medium supplemented with 50 ng/mL recombinant human NF-κB ligand (RANKL; Peprotech) for 8 days [20]. The cultures were replenished with fresh medium containing growth factors every 3 days. On day 8, the cells were fixed with 4% paraformaldehyde (Wako) and stained with a leukocyte acid phosphate TRAP kit (Sigma), and actin ring staining was performed with Alexa Fluor 633 phalloidin (Invitrogen, Carlsbad, CA) and DAPI (Dojindo Molecular Technologies). For the functional assay, monocytes were cultured on thin-type dentin slices from Ivory (Wako, Japan) for 21 days in the same medium containing growth factors [21]. Bone resorption pits were stained with a 20 mg/ml solution of peroxidase-conjugated wheat germ agglutinin (Sigma) and 3,3′-diaminobenzidine (0.52 mg/mL in PBS containing 0.1% H2O2) and examined via confocal microscopy (BZ-

X710, KEYENCE, Japan). Images were analyzed via ImageJ (NIH, USA) to determine the size of bone resorption pits. For co-culturing FLSs with osteoclast precursors, human monocytes were purified, seeded onto 24-well plate ($1X10^5$) and cultured in the presence of recombinant hMCSF (Peprotech) for 3 days. In parallel, hFLSs (Cell Applications, USA), were placed ($1X10^5$) in transwell inserts (1.0 μm Falcon cell culture inserts, BD, USA) and cultured in growth medium containing TNFα (10ng/mL) for 24h. Supernatant was harvested, centrifuged to remove cell debris and kept in -80 °C for further analysis. Thereafter, the FLSs and monocytes (osteoclast precursors) were washed with ice-cold PBS, and transwell inserts were placed on 24-well plate, and cultured together for 7 days [21]. Monocytes were then stained with a leukocyte acid phosphate TRAP kit (Sigma).

2.4.Quantitative real-time polymerase chain reaction

Cultured cells were lysed via TRIzol Reagent (Invitrogen) for RNA extraction. DNA-free RNA was purified via the RNeasy Plus Mini kit column (Qiagen), and 0.5 μg of RNA was reverse transcribed via the GoScriptTM reverse transcriptase kit (Promega, USA) to generate cDNAs. The prepared cDNAs were assayed via SYBR Premix Ex TaqTM II (Takara) with primers specific for each gene (Supplementary Table 1) via a Thermal Cycler Dice (Real-Time System II, Takara, Japan). Gene expression levels were calculated after normalization to the expression of the reference gene via the $2^{-\Delta\Delta Ct}$ method[20].

2.5. Western blotting

Cultured cells were lysed, and the extracted proteins were subjected to standard procedures for SDS–PAGE and Western blot analysis (ATTO, Tokyo, Japan). Bands on

polyvinylidene fluoride membranes (Immobilon-P Membrane; Merck, Darmstadt, Germany) were detected via target-specific primary antibodies (Supplementary Table 2) and corresponding secondary HRP-conjugated antibodies (CST, MA, USA), followed by treatment with solutions from the Ez WestLumi Plus Kit (ATTO). The images were visualized via an iBright 1500 Imaging System (Thermo Fisher Scientific, Inc., USA), and the relative intensities of the bands were quantified on the basis of the density of each target to the band density of β-actin (ImageJ, NIH).

2.6.Senescent cells staining

Cultured cells stimulated with recombinant CCN3 for 168 h were fixed and stained with a senescence β-galactosidase staining kit (Cell Signaling, Massachusetts, USA). Images were examined via confocal microscopy (BZ-X710, KEYENCE), and the percentage of β-galactosidase-stained cells (ImageJ, NIH) was analyzed.

2.7.RNA-sequencing and bioinformatics

High-quality RNA samples (3 samples for each condition) were used to generate the libraries via the NEBNext Ultra II Directional RNA Library Prep Kit (MA, USA). Only high-quality libraries were subjected to Illumina NovaSeq 6000 (Illumina) sequencing, and the sequence data of 150 bp × 2 paired ends of 4–6G bases/sample were trimmed quickly and mapped via HISAT2 v2.0.5. The reads were quantified via RSEM, and the raw count data were subjected to the edgeR R package (3.22.5) to determine the differentially expressed genes (DEGs) and fold changes. Significance was set up on the basis of a < 0.05 false discovery rate (FDR). Gene Ontology (GO) and pathway enrichment analyses were

performed via the public database for the gene-set enrichment tool ShinyGO (http://bioinformatics.sdstate.edu/go74/), and visualization/graphing was performed via SRplot tools (http://www.bioinformatics.com.cn/srplot) (Tang et al., 2023). BBrowserX software (BioTuring Inc., San Diego, CA, USA: https://bioturing.com/bbrowserx) was used for analyzing single-cell RNA-sequencing (scRNA-Seq) public databases. The RNA-seq data reported in this study are deposited in the Gene Expression Omnibus (GEO) database (https://www.ncbi.nlm.nih.gov/geo/) with the accession numbers GSE271643, GSE171542, and GSE272743. Other public databases used in the current study include GSE129087 and GSE100191.

*2.8.*In vivo *stimulation assays*

To understand the effects of CCN3 in vivo, 2 models were used with different administration methods. Recombinant murine CCN3 (R&D system) was administered via the implantation of a 1 cm × 1 cm sponge (PELNAC, Tokyo, Japan) soaked in 50 μL of PBS containing 4 μg of recombinant mouse CCN3 onto the calvarial bone of 10-week-old BALB/cAJc1 mice (CLEA). This model allows direct interaction between the molecules and bone as sponges slowly release CCN3 over the calvarial bones. The skulls where the sponge was implanted were harvested on day 4 for gene expression analysis and day 7 for bone histomorphometry analysis [22]. The fixed calvariae were subjected to high-resolution micro computed tomography (micro-CT) scanning R_mCT2 (Rigaku, Tokyo, Japan) at a 10-mm isotropic resolution. The percentage of bone pits on the surface of the calvariae was calculated via ImageJ (NIH). Next, the 10% formalin-fixed samples were decalcified in 10% EDTA (Wako, Osaka, Japan) for 3 days and embedded in paraffin. Five-micron-thick

sections were prepared, stained with hematoxylin and eosin, and subjected to tartrate resistance acid phosphatase (TRAP) staining. The lesions and infiltration of TRAP-positive cells were microscopically examined, and images were analyzed with ImageJ (NIH). In a separate experiment, recombinant murine CCN3 (R&D system) was administered into the left knee joints of 10-week-old BALB/cAJc1 mice (CLEA, Tokyo, Japan). The injections were performed three times a week (2-day intervals), and on the seventh day, the knee joints were harvested, decalcified with EDTA, embedded in paraffin, and stained for histological examination. Sections were stained with HE and an antibody against P53 (GeneTex, California, USA). P53-positive cells in the synovium of the sectioned tissues were counted.

2.9. Collagen antibody-induced arthritis (CAIA) model

Ten-week-old BALB/cAJc1 mice (CLEA) were intravenously injected via the tail vein with 4 mg of an Arthritis-inducing Monoclonal Antibody Cocktail (Cosmo Bio, Tokyo, Japan), followed by intraperitoneal injection of 50 μg (100 μl) of lipopolysaccharide (LPS; Sigma) on day 3 [23]. On day 3, the mice were randomly divided into two groups: a test group, which received intraperitoneal injections of 40 μg (100 μl) anti-CCN3 antibody (Bio-Techne, Minneapolis, USA), and a control group, which received 40 μg (100 μl) of the isotype IgG antibody (Bio-Techne, Minneapolis, USA). The injections were repeated twice a week throughout the period of the experiment. The limbs of the mice were observed every day, and the severity of arthritis was scored from 0 to 4 points as follows: 0: no inflammation in any joint (finger, back, wrist or ankle); 1: inflammation in one joint; 2: inflammation in the two joints; 3: inflammation in all joints; and 4: severe swelling in all joints), with a maximum of 16 points for all four limbs. On days 14 and 28, the right hind paws were

collected, decalcified with EDTA (Wako, Japan), embedded in paraffin, and stained with HE and TRAP. The inflammatory cell infiltration area (within a 3 × 2 mm area) and the percentage of the TRAP-positive area in the TRAP-stained sections were determined via ImageJ (NIH, USA).

2.10. Statistical analysis

Statistical analyses were performed via GraphPad Software Prism 9 (CA, USA), with tests including one-way ANOVA followed by Tukey's multiple comparisons procedure (multiple groups) and an unpaired Student's t test (two groups). The results were considered statistically significant when *$p < 0.05$, **$p < 0.001$, ***$p < 0.0001$, and ****$p < 0.00001$; ns indicates no significant difference. The error bars indicate the SEM.

3. RESULTS

3.1. Detection of CCN3 in RA synovial tissues and inflammatory subsets of fibroblasts

To first confirm the expression of CCN3 in synovial tissues, immunostaining was performed with a specific antibody in synovial tissues collected from RA patients. Strong signals of CCN3-positive cells were observed in the synovial tissues of the RA knee and wrist (Fig. 1A & Supplementary Fig. 1). To further gain additional evidence of the expression of CCN3 in synovial tissues, public scRNA-seq data were analyzed to trace the expression of CCN3. Human RA synoviocytes (375 cells) [24] included 110 CCN3-positive cells, and the majority of the cells were clustered in an inflammatory subset expressing the FAPα marker (Fig. 1B, C). Consistent with these results, analysis of database from experimental mouse RA joints [25] revealed that Ccn3 is expressed in 844 of 4732 cells in the whole synovial joint,

and the majority of the positive cells were positive for the inflammatory synoviocyte marker FAPα (Fig. 1C, D). These results revealed that CCN3 is expressed in the synovial tissue of RA joints, mainly in the inflammatory fibroblast subset.

3.2. CCN3 stimulation results in the activation of the senescence pathway in synoviocytes in vitro and in vivo

To explore the role of CCN3 in RA, human fibroblast-like synoviocytes (FLSs) were cultured, stimulated with recombinant CCN3 for 24 h and then subjected to bulk RNA-seq analysis. A total of 349 genes were significantly upregulated in CCN3-stimulated FLSs, and these genes were enriched in the TGF-β signaling, Hippo signaling, osteoclast differentiation and lysosome pathways (Fig. 2A, B). GO enrichment analysis revealed that this stimulation resulted in the upregulation of genes involved in the collagen metabolic process for the biological process and growth factor binding for the molecular function (Fig. 2C, D). Transcriptional regulatory network enrichment analysis revealed that the upregulated genes were significantly enriched in the tumor protein p53 (p=0.0342). The genes enriched in the TP53 term included ADGRB1, HSF1, ID1, KLF, TP53I3, PCBP4, and ZNF385A (Fig. 2E). Among these genes, PCBP4 and ZNF385A are known to play essential roles in cellular senescence. Venn analysis revealed that 20 genes whose expression was upregulated in CCN3-stimulated FLSs were highly expressed in aging cells and were associated with cellular senescence (Fig. 2F, G). Similarly, the increased gene expression of SASP genes in CCN3-stimulated FLSs was confirmed by qRT–PCR (Supplementary Fig. 2). Extending the stimulation period with CCN3 to 168 h resulted in a significant increase in the protein expression of β-galactosidase (β-gal), P53 and P21 as well as the number of β-gal-positive

FLSs in the cultures (Fig. 2H, I). To further elucidate the role of CCN3 in the activation of cellular senescence, we injected CCN3 into the knee joint and examined the number of p53- and β-gal-positive cells after 7 days. Our results revealed a significant increase in the percentage of p53-positive cells in the synovium of knees injected with murine recombinant CCN3 joints compared with those in PBS-injected mice (Fig. 3A–C). These collective findings suggest that CCN3 activates the senescence pathway in synoviocytes, resulting in the development of inflammation in the joints.

3.3. CCN3 stimulation promotes osteoclastogenesis in vitro and in vivo

The results demonstrated that stimulating FLSs with CCN3 resulted in increased expression of NFATc1 and AP1, which are the major transcription factors involved in osteoclast differentiation, raising the question of whether CCN3 can induce osteoclast differentiation. Human monocytes were stimulated with CCN3 for 8 days and then stained with TRAP and actin ring for morphological evaluation. For their bone-resorbing activity, human monocytes were cultured on dentin slices and stimulated with CCN3 for 21 days. Importantly, stimulation with CCN3 led to the development of osteoclast-like cells with modest bone-resorbing activity in vitro (Fig. 4A-C). Gene expression analysis of osteoclast-like cells induced by CCN3 stimulation revealed that the genes whose expression was upregulated (315 genes) were the most significantly enriched in cellular senescence, osteoclast differentiation and the regulation of telomerase activity according to the KEGG pathway and biological process enrichment analyses (Fig. 4D-G & Supplementary Figure 3). These genes were also significantly enriched in the cell cycle ($p=0.00237$), TGF-β signaling ($p=0.00364$), and focal adhesion ($p=0.0149$) pathways (Fig. 4H, I). Importantly,

transcriptional regulatory network enrichment analysis demonstrated that the upregulated genes were most significantly enriched in SP1, FOS RB1 and TP53 (Fig. 4J). These results revealed that CCN3 stimulation led to the activation of signaling pathways that are involved in the development of senescence and osteoclastogenesis in monocyte/macrophages. In support of these results, stimulation of human macrophages with CCN3 for 168 h (in the absence of recombinant MCSF) resulted in a significant increase in β-gal-positive cells in vitro (Fig. 4K). In line with these results, co-culturing TNF-α-stimulated FLS with monocytes for 7 days resulted in an increase of $TRAP^+$ cells as compared to these cultured with non-stimulated FLS (Supplementary Figure 3). The increase of $TRAP^+$ cells was associated with an elevation in the level of CCN3 in the supernatant of the TNF-α-stimulated FLS (Supplementary Figure 4). To further verify our in vitro findings, CCN3-soaked sponges were transplanted onto the calvariae for 7 days, and histological and histomorphometric analyses were performed on day 7 (Fig. 5A). Larger bone resorption and TRAP-stained areas were observed in the mice that received the CCN3-soaked sponges than in those that received the PBS-soaked sponges (Fig. 5B-C). Notably, these mice presented a significant increase in the number of pP53- and β-gal-positive cells around the transplanted soaked sponges (Fig. 5D). Similarly, mice that received CCN3-soaked sponges presented increased expression of TNFα, IL-7, and MMP3, which are related to SASP, in calvarial bone harvested 4 days after transplantation (Supplementary Fig. 5). These results indicate that CCN3 can promote osteoclastogenesis and SASP, which lead to the development of bone erosion and inflammation in the joints.

3.4. Therapeutic effects of CCN3 blockade in a CAIA model

Given that CCN3 can promote pathways involved in senescence and osteoclast differentiation, which are hallmark characteristics/features of RA joints, we investigated the usefulness of targeting CCN3 in an RA mouse model. RA symptoms were induced by the administration of an arthritis-inducing monoclonal antibody cocktail and LPS, and treatment with a specific antibody against murine CCN3 was performed (Fig. 6A). The limbs of the mice were observed daily for assessment of arthritis clinical scores, and the right hind paws were collected on days 14 and 28 for histological examination. The administration of the CCN3 antibody significantly reduced the arthritis clinical and inflammation scores (Fig. 6B-D). In line with these results, this treatment significantly reduced the number of β-gal-positive cells and the TRAP-stained area in the sectioned tissues harvested on days 14 and 28, respectively (Fig. 6E). Taken together, the beneficial effects of targeting CCN3 in vivo highlight it as a new molecular target for the treatment of RA.

4. DISCUSSION

Despite recent advances in our knowledge of the pathogenesis of RA, many issues remain to be resolved [26]. In fact, recent evidence revealing the mechanism of senescence should provide solid clues for the discovery of new therapeutic strategies for autoimmune diseases, including RA [10]. These findings raised the question of whether targeting factors mediating/inducing senescence in the joint can prevent the progression of the RA process. Here, a senescence-related molecule, CCN3, which has been found in RA joints and blood patients and is associated with disease severity [18][19][27], was studied as a target for the treatment of RA.

Our results demonstrated that CCN3 contributed to the pathophysiology of RA by activating the senescence pathway in synoviocytes and promoting osteoclast differentiation in their precursor cells. In line with our findings, transgenic mice with CCN3 overexpression in articular cartilage exhibit characteristic features of senescence in chondrocytes and severe degenerative changes in cartilage. Moreover, treating chondrocytes with recombinant CCN3 resulted in an increase in the expression of P21 and P53 [12]. In contrast to these findings, CCN3 administration ameliorates cartilage catabolism in IL-1β-induced osteoarthritis by inhibiting the activation of the PI3K/AKT/mTOR pathway and promoting chondrocyte autophagy [28]. The ability of CCN3 to activate cyclin-dependent kinase inhibitors has been reported in smooth muscle cells in a manner dependent on Notch signaling [29]. On the other hand, our data revealed that recombinant CCN3 promoted genes involved in TGF-β signaling in macrophages and synoviocytes. A convincing body of evidence shows that TGF-β signaling is involved in the activation of senescence pathways via interactions with cyclin-dependent kinase inhibitors [30][31]. Therefore, the ability of CCN3 to induce senescence in tissue provides a possible explanation for the association between inflammatory cytokine production and increased levels of CCN3 in blood and tissues [15]. Similarly, the presence of CCN3 in the joint promotes the senescence-associated secretory phenotype (SASP) in synoviocyte cells, resulting in the development of chronic inflammation that accelerates the senescence of immune cells and creates a vicious cycle of inflammation and senescence.

Furthermore, a wealth of data also supports the notion that CCN3 plays a critical role in bone remodeling and osteolytic bone metastases [32][33]. Compared with WT mice, transgenic mice overexpressing CCN3 presented a decrease in trabecular bone volume, with

no change in osteoblast or osteoclast numbers. Overexpressing CCN3 in the ST-2 stromal cell line and recombinant CCN3 at high concentrations (300–600 ng/mL) inhibited osteoblast differentiation in vitro via the BMP and Notch signaling pathways [34]. Son and colleagues reported that CCN3 activates the Wnt/β-catenin/MITF signaling axis, thereby activating EGFR signaling, which promotes metastasis and tumor progression in breast cancer [16]. In prostate cancer, CCN3 promotes VEGF-dependent angiogenesis via the activation of focal adhesion kinase (FAK)/AKT/NF-κB signaling in endothelial progenitor cells [35]. However, another study demonstrated that CCN3 has a negative effect on NF-κB signaling, which is needed for the activation of endothelial cells and the production of inflammatory cytokines [36].

Another important finding from our study is that CCN3 stimulation resulted in the formation of osteoclast-like cells that have the ability to resorb bone. This stimulation was accompanied by an increase in the expression of integrins in monocytes. In agreement with our findings, CCN3 seems to interact with and activate integrins, including αvβ3 and α5β1, in endothelial cells to promote cell adhesion, migration, and angiogenesis [37]. Likewise, CCN3 has been implicated in cutaneous wound healing via the activation of integrins in fibroblasts [38]. Integrins, namely, αvβ3 integrins, are important transduction molecules that play essential roles in osteoclastogenesis by facilitating the adhesion and migration of osteoclast precursors and sealing zones to form the required cytoskeletal structure of osteoclasts [39]. Therefore, the formation of osteoclast-like cells after CCN3 stimulation is most likely due to its ability to activate integrins that mediate cell adhesion and fusion. On the other hand, our RNA-seq data showed that CCN3 stimulation activated TGF-β signaling

which is involved in activation of non-canonical pathway of osteoclastogenesis [40]. Collectively, these findings show that CCN3 can activate different transcription factors that are involved in multiple biological processes, including cell senescence, adhesion, differentiation and angiogenesis, making this molecule a promising target for RA treatment.

Furthermore, our data demonstrated that systemic treatment with an antibody against CCN3 improved clinical symptoms and reduced inflammation in synovial tissues and the number of senescent cells as well as osteoclasts in the joint. These are consistent with findings reported by Marchal and colleagues, who identified CCN3 as a promising target for the treatment of renal diseases, as the inhibition of CCN3 limits inflammatory cell infiltration and renal interstitial fibrosis [41]. A wealth of evidence highlights that CCN proteins are attractive therapeutic targets in diverse diseases, such as chronic inflammatory diseases, interstitial lung disease, chronic kidney disease, hepatic fibrosis and cancer[42]. Importantly, CCN2 has been documented as a therapeutic target for pulmonary fibrosis, and its antibody (FG-3019) has been clinically used and has achieved significant therapeutic effects in patients with idiopathic pulmonary fibrosis [43].

In conclusion, our results suggest that CCN3 acts as an autocrine/paracrine factor that contributes to the activation of cellular senescence and osteoclastogenesis in joints and that systemic blockade of this molecule is associated with a reduction in inflammation and bone resorption in an experimental RA model. Our collective data shed light on an attractive target for the treatment of RA.

Conflicts of interest

All the authors state that they have no conflicts of interest.

Data availability

The data in this study are available within the article and supplementary information. The RNA-seq data related to this study are publicly available in the Gene Expression Omnibus (GEO) database (https://www.ncbi.nlm.nih.gov/geo/). Other data will be made available upon reasonable request.

Funding

This work was supported by research grants from the Japan Society for the Promotion of Science (Grant-in-Aid for Early-Career Scientists; 23K15704), the Japan Agency for Medical Research and Development (Moonshot Research and Development Program, PJ4221KB01), and the Kobayashi Foundation.

References

[1] E.M. Gravallese, G.S. Firestein, Rheumatoid Arthritis — Common Origins, Divergent Mechanisms, New England Journal of Medicine 388 (2023) 529–542. https://doi.org/10.1056/nejmra2103726.

[2] T.K. Gill, M.M. Mittinty, L.M. March, J.D. Steinmetz, G.T. Culbreth, M. Cross, J.A. Kopec, A.D. Woolf, L.M. Haile, H. Hagins, K.L. Ong, D.R. Kopansky-Giles, K.E. Dreinhoefer, N. Betteridge, M. Abbasian, M. Abbasifard, K. Abedi, M.A. Adesina, J.P. Aithala, M. Akbarzadeh-Khiavi, Y. Al Thaher, T.A. Alalwan, H. Alzahrani, S. Amiri, B. Antony, J. Arabloo, A.Y. Aravkin, A. Arumugam, K.K. Aryal, S.S. Athari, A. Atreya, S. Baghdadi, M. Bardhan, L.H. Barrero, L.M. Bearne, A.B. Bekele, I.M. Bensenor, P. Bhardwaj, R. Bhatti, A. Bijani, T. Bordianu, S. Bouaoud, A.M. Briggs, H.A. Cheema, S.W.M.P. Christensen, I.S. Chukwu, B. Clarsen, X. Dai, K. de Luca, B. Desye, M. Dhimal, T.C. Do, A.F. Fagbamigbe, S.F. Forghani, N. Ferreira, B. Ganesan, M. Gebrehiwot, A. Ghashghaee, S.M. Graham, N.I. Harlianto, J. Hartvigsen, A.I. Hasaballah, M. Hasanian, M.B. Hassen, S.I. Hay, M. Heidari, A.K. Hsiao, I.M. Ilic, M. Jokar, H. Khajuria, M.J. Khan, P. Khanal, S. Khateri, A. Kiadaliri, M.S. Kim, A. Kisa, A.A. Kolahi, K. Krishan, V. Krishnamoorthy, I. Landires, B.

Larijani, T.T.T. Le, Y.H. Lee, S.S. Lim, J. Lo, S.P. Madani, J.N. Malagón-Rojas, I. Malik, H.R. Marateb, A.J. Mathew, T.J. Meretoja, M.K. Mesregah, T. Mestrovic, A. Mirahmadi, A. Misganaw, S. Mohaghegh, A.H. Mokdad, K. Momenzadeh, S. Momtazmanesh, L. Monasta, M.A. Moni, Y. Moradi, E. Mostafavi, J.S. Muhammad, C.J.L. Murray, S. Muthu, S. Nargus, H. Nassereldine, S. Neupane, R.K. Niazi, I.H. Oh, H. Okati-Aliabad, A. Oulhaj, K. Pacheco-Barrios, S. Park, J. Patel, S. Pawar, P. Pedersini, M.F.P. Peres, I.R. Petcu, F.E. Petermann-Rocha, M. Poursadeqiyan, I. Qattea, M.F. Qureshi, Q. Rafferty, S. Rahimi-Dehgolan, M. Rahman, S.K. Ramasamy, V. Rashedi, E.M.M. Redwan, D.C. Ribeiro, L. Roever, A. Safary, D. Sagoe, F.S. Sharif-Askari, A. Sahebkar, S. Salehi, A. Shafaat, S. Shahabi, S. Sharma, B.B. Shashamo, R. Shiri, A. Singh, H. Slater, A.E. Smith, D.R. Sunuwar, M. Tabish, S. Tharwat, I. Ullah, S.V. Tahbaz, T.J. Vasankari, J.H. Villafañe, S.E. Vollset, T. Wiangkham, N. Yonemoto, Y. You, I. Zare, P. Zheng, T. Vos, P.M. Brooks, Global, regional, and national burden of other musculoskeletal disorders, 1990–2020, and projections to 2050: a systematic analysis of the Global Burden of Disease Study 2021, Lancet Rheumatol 5 (2023) e670–e682. https://doi.org/10.1016/S2665-9913(23)00232-1.

[3] A.M.H. Boots, A.B. Maier, P. Stinissen, P. Masson, R.J. Lories, F. De Keyser, The influence of ageing on the development and management of rheumatoid arthritis, Nat Rev Rheumatol 9 (2013) 604–613. https://doi.org/10.1038/nrrheum.2013.92.

[4] J.M. Bathon, R.M. Fleischmann, D.M. Van Der Heijde, J.R. Tesser, P.M. Peloso, Y. Chon, B. White, J.M. Bathon, Safety and Efficacy of Etanercept Treatment in Elderly Subjects with Rheumatoid Arthritis, 2006. www.jrheum.org.

[5] B.J. Radovits, W. Kievit, J. Fransen, M.A.F.J. Van De Laar, T.L. Jansen, P.L.C.M. Van Riel, R.F.J.M. Laan, Influence of age on the outcome of antitumour necrosis factor alpha therapy in rheumatoid arthritis, Ann Rheum Dis 68 (2009) 1470–1473. https://doi.org/10.1136/ard.2008.094730.

[6] R. Holmdahl, V. Malmström, H. Burkhardt, Autoimmune priming, tissue attack and chronic inflammation - The three stages of rheumatoid arthritis, Eur J Immunol 44 (2014) 1593–1599. https://doi.org/10.1002/eji.201444486.

[7] M.J. Del Rey, Á. Valín, A. Usategui, S. Ergueta, E. Martín, C. Municio, J.D. Cañete, F.J. Blanco, G. Criado, J.L. Pablos, Senescent synovial fibroblasts accumulate prematurely in rheumatoid arthritis tissues and display an enhanced inflammatory phenotype, Immunity and Ageing 16 (2019). https://doi.org/10.1186/s12979-019-0169-4.

[8] B. Bartok, G.S. Firestein, Fibroblast-like synoviocytes: Key effector cells in rheumatoid arthritis, Immunol Rev 233 (2010) 233–255. https://doi.org/10.1111/j.0105-2896.2009.00859.x.

[9] I.A. Udalova, A. Mantovani, M. Feldmann, Macrophage heterogeneity in the context of rheumatoid arthritis, Nat Rev Rheumatol 12 (2016) 472–485. https://doi.org/10.1038/nrrheum.2016.91.

[10] N.S. Gasek, G.A. Kuchel, J.L. Kirkland, M. Xu, Strategies for targeting senescent cells in human disease, Nat Aging 1 (2021) 870–879. https://doi.org/10.1038/s43587-021-00121-8.

[11] K. Hirose, M. Kuwahara, E. Nakata, T. Tetsunaga, K. Yamada, K. Saiga, M. Takigawa, T. Ozaki, S. Kubota, T. Hattori, Elevated Expression of CCN3 in Articular Cartilage Induces Osteoarthritis in Hip Joints Irrespective of Age and Weight Bearing, Int J Mol Sci 23 (2022). https://doi.org/10.3390/ijms232315311.

[12] M. Kuwahara, K. Kadoya, S. Kondo, S. Fu, Y. Miyake, A. Ogo, M. Ono, T. Furumatsu, E. Nakata, T. Sasaki, S. Minagi, M. Takigawa, S. Kubota, T. Hattori, Ccn3 (Nov) drives degradative changes in aging articular cartilage, Int J Mol Sci 21 (2020) 1–18. https://doi.org/10.3390/ijms21207556.

[13] J. Pakradouni, W. Le Goff, C. Calmel, B. Antoine, E. Villard, E. Frisdal, M. Abifadel, J. Tordjman, C. Poitou, D. Bonnefont-Rousselot, R. Bittar, E. Bruckert, K. Clément, B. Fève, C. Martinerie, M. Guérin, Plasma NOV/CCN3 Levels Are Closely Associated with Obesity in Patients with Metabolic Disorders, PLoS One 8 (2013). https://doi.org/10.1371/journal.pone.0066788.

[14] C. Martinerie, M. Garcia, T.T.H. Do, B. Antoine, M. Moldes, G. Dorothee, C. Kazazian, M. Auclair, M. Buyse, T. Ledent, P.O. Marchal, M. Fesatidou, A. Beisseiche, H. Koseki, S. Hiraoka, C.E. Chadjichristos, B. Blondeau, R.G. Denis, S. Luquet, B. Fève, NOV/CCN3: A new adipocytokine involved in obesity-associated insulin resistance, Diabetes 65 (2016) 2502–2515. https://doi.org/10.2337/db15-0617.

[15] A. Fadhil Jaafar, R. Afrisham, R. Fadaei, V. Farrokhi, N. Moradi, A. Abbasi, N. Einollahi, CCN3/NOV serum levels in coronary artery disease (CAD) patients and its correlation with TNF-α and IL-6, BMC Res Notes 16 (2023). https://doi.org/10.1186/s13104-023-06590-x.

[16] S. Son, H. Kim, H. Lim, J. hyung Lee, K. min Lee, I. Shin, CCN3/NOV promotes metastasis and tumor progression via GPNMB-induced EGFR activation in triple-negative breast cancer, Cell Death Dis 14 (2023). https://doi.org/10.1038/s41419-023-05608-3.

[17] N. Saleem Zayed, Association Of Cellular Communication Network Factor 3 (CCN3) With Rheumatoid Arthritis Disease And It's Severity (Case-Control Study), Medical Science Journal for Advance Research 3 (2022) 201–208. https://doi.org/10.46966/msjar.v3i4.85.

[18] N. Macías-Segura, J.E. Castañeda-Delgado, Y. Bastian, D. Santiago-Algarra, J.D. Castillo-Ortiz, A.L. Alemán-Navarro, E. Jaime-Sánchez, M. Gomez-Moreno, C.A. Saucedo-Toral, E.E. Lara-Ramírez, M. Zapata-Zuñiga, L. Enciso-Moreno, R. González-Amaro, C. Ramos-Remus, J.A. Enciso-Moreno, Transcriptional signature associated with early rheumatoid arthritis and healthy individuals at high risk to develop the disease, PLoS One 13 (2018). https://doi.org/10.1371/journal.pone.0194205.

[19] Y. Wei, L. Peng, Y. Li, N. Zhang, K. Shang, L. Duan, J. Zhong, J. Chen, Higher Serum CCN3 Is Associated with Disease Activity and Inflammatory Markers in Rheumatoid Arthritis, J Immunol Res 2020 (2020). https://doi.org/10.1155/2020/3891425.

[20] Y. Tian, M.A. Terkawi, T. Onodera, H. Alhasan, G. Matsumae, D. Takahashi, M. Hamasaki, T. Ebata, M.K. Aly, H. Kida, T. Shimizu, K. Uetsuki, K. Kadoya, N. Iwasaki, Blockade of XCL1/Lymphotactin Ameliorates Severity of Periprosthetic Osteolysis Triggered by Polyethylene-Particles, Front Immunol 11 (2020) 1720. https://doi.org/10.3389/fimmu.2020.01720.

[21] S. Yokota, G. Matsumae, T. Shimizu, T. Hasegawa, T. Ebata, D. Takahashi, C. Heguo, Y. Tian, H. Alhasan, M. Takahata, K. Kadoya, M.A. Terkawi, N. Iwasaki, Cardiotrophin Like Cytokine Factor 1 (CLCF1) alleviates bone loss in osteoporosis mouse models by suppressing osteoclast differentiation through activating interferon signaling and repressing the nuclear factor-κB signaling pathway, Bone 153 (2021). https://doi.org/10.1016/j.bone.2021.116140.

[22] G. Matsumae, T. Shimizu, Y. Tian, D. Takahashi, T. Ebata, H. Alhasan, S. Yokota, K. Kadoya, M.A. Terkawi, N. Iwasaki, Targeting thymidine phosphorylase as a potential therapy for bone loss associated with periprosthetic osteolysis, Bioeng Transl Med 6 (2021). https://doi.org/10.1002/btm2.10232.

[23] T. Endo, K. Ito, J. Morimoto, M. Kanayama, D. Ota, M. Ikesue, S. Kon, D. Takahashi, T. Onodera, N. Iwasaki, T. Uede, Syndecan 4 regulation of the development of autoimmune arthritis in mice by modulating B cell migration and germinal center formation, Arthritis and Rheumatology 67 (2015) 2512–2522. https://doi.org/10.1002/art.39193.

[24] F. Mizoguchi, K. Slowikowski, K. Wei, J.L. Marshall, D.A. Rao, S.K. Chang, H.N. Nguyen, E.H. Noss, J.D. Turner, B.E. Earp, P.E. Blazar, J. Wright, B.P. Simmons, L.T. Donlin, G.D. Kalliolias, S.M. Goodman, V.P. Bykerk, L.B. Ivashkiv, J.A. Lederer, N. Hacohen, P.A. Nigrovic, A. Filer, C.D. Buckley, S. Raychaudhuri, M.B. Brenner, Functionally distinct disease-associated fibroblast subsets in rheumatoid arthritis, Nat Commun 9 (2018). https://doi.org/10.1038/s41467-018-02892-y.

[25] A.P. Croft, J. Campos, K. Jansen, J.D. Turner, J. Marshall, M. Attar, L. Savary, C. Wehmeyer, A.J. Naylor, S. Kemble, J. Begum, K. Dürholz, H. Perlman, F. Barone, H.M. McGettrick, D.T. Fearon, K. Wei, S. Raychaudhuri, I. Korsunsky, M.B. Brenner, M. Coles, S.N. Sansom, A. Filer, C.D. Buckley, Distinct fibroblast subsets drive inflammation and damage in arthritis, Nature 570 (2019) 246–251. https://doi.org/10.1038/s41586-019-1263-7.

[26] V. Strand, R. Kimberly, J.D. Isaacs, Biologic therapies in rheumatology: Lessons learned, future directions, Nat Rev Drug Discov 6 (2007) 75–92. https://doi.org/10.1038/nrd2196.

[27] M. Armaka, D. Konstantopoulos, C. Tzaferis, M.D. Lavigne, M. Sakkou, A. Liakos, P.P. Sfikakis, M.A. Dimopoulos, M. Fousteri, G. Kollias, Single-cell multimodal

analysis identifies common regulatory programs in synovial fibroblasts of rheumatoid arthritis patients and modeled TNF-driven arthritis, Genome Med 14 (2022). https://doi.org/10.1186/s13073-022-01081-3.

[28] X. Huang, B. Ni, Z. Mao, Y. Xi, X. Chu, R. Zhang, X. Ma, H. You, NOV/CCN3 induces cartilage protection by inhibiting PI3K/AKT/mTOR pathway, J Cell Mol Med 23 (2019) 7525–7534. https://doi.org/10.1111/jcmm.14621.

[29] T. Shimoyama, S. Hiraoka, M. Takemoto, M. Koshizaka, H. Tokuyama, T. Tokuyama, A. Watanabe, M. Fujimoto, H. Kawamura, S. Sato, Y. Tsurutani, Y. Saito, B. Perbal, H. Koseki, K. Yokote, CCN3 inhibits neointimal hyperplasia through modulation of smooth muscle cell growth and migration, Arterioscler Thromb Vasc Biol 30 (2010) 675–682. https://doi.org/10.1161/ATVBAHA.110.203356.

[30] S. Ueda, T. Tominaga, A. Ochi, A. Sakurai, K. Nishimura, E. Shibata, S. Wakino, M. Tamaki, K. Nagai, TGF-β1 is involved in senescence-related pathways in glomerular endothelial cells via p16 translocation and p21 induction, Sci Rep 11 (2021). https://doi.org/10.1038/s41598-021-01150-4.

[31] S. Matsuda, A. Revandkar, T.D. Dubash, A. Ravi, B.S. Wittner, M. Lin, R. Morris, R. Burr, H. Guo, K. Seeger, A. Szabolcs, D. Che, L. Nieman, G.A. Getz, D.T. Ting, M.S. Lawrence, J. Gainor, D.A. Haber, S. Maheswaran, TGF-β in the microenvironment induces a physiologically occurring immune-suppressive senescent state, Cell Rep 42 (2023). https://doi.org/10.1016/j.celrep.2023.112129.

[32] V. Ouellet, P.M. Siegel, CCN3 modulates bone turnover and is a novel regulator of skeletal metastasis, J Cell Commun Signal 6 (2012) 73–85. https://doi.org/10.1007/s12079-012-0161-7.

[33] M. Dankner, V. Ouellet, L. Communal, E. Schmitt, D. Perkins, M.G. Annis, V. Barrès, C. Caron, A.M. Mes-Masson, F. Saad, P.M. Siegel, CCN3/Nephroblastoma Overexpressed Is a Functional Mediator of Prostate Cancer Bone Metastasis That Is Associated with Poor Patient Prognosis, American Journal of Pathology 189 (2019) 1451–1461. https://doi.org/10.1016/j.ajpath.2019.04.006.

[34] S. Rydziel, L. Stadmeyer, S. Zanotti, D. Durant, A. Smerdel-Ramoya, E. Canalis, Nephroblastoma overexpressed (Nov) inhibits osteoblastogenesis and causes osteopenia, Journal of Biological Chemistry 282 (2007) 19762–19772. https://doi.org/10.1074/jbc.M700212200.

[35] P.-C. Chen, H.-C. Cheng, J. Wang, S.-W. Wang, H.-C. Tai, C.-W. Lin, C.-H. Tang, Prostate cancer-derived CCN3 induces M2 macrophage infiltration and contributes to angiogenesis in prostate cancer microenvironment, n.d. www.impactjournals.com/oncotarget/.

[36] Z. Lin, V. Natesan, H. Shi, A. Hamik, D. Kawanami, C. Hao, G.H. Mahabaleshwar, W. Wang, Z.G. Jin, G.B. Atkins, S.M. Firth, L. Rittié, B. Perbal, M.K. Jain, A novel role of CCN3 in regulating endothelial inflammation, J Cell Commun Signal 4 (2010) 141–153. https://doi.org/10.1007/s12079-010-0095-x.

[37] C.G. Lin, S.J. Leu, N. Chen, C.M. Tebeau, S.X. Lin, C.Y. Yeung, L.F. Lau, CCN3 (NOV) is a novel angiogenic regulator of the CCN protein family, Journal of Biological Chemistry 278 (2003) 24200–24208. https://doi.org/10.1074/jbc.M302028200.
[38] C.G. Lin, C.C. Chen, S.J. Leu, T.M. Grzeszkiewicz, L.F. Lau, Integrin-dependent functions of the angiogenic inducer NOV (CCN3): Implication in wound healing, Journal of Biological Chemistry 280 (2005) 8229–8237. https://doi.org/10.1074/jbc.M404903200.
[39] L.T. Duong, P. Lakkakorpi, I. Nakamura, G.A.R. Rodan¨, Mini Review Integrins and signaling in osteoclast function, 2000.
[40] Y. Xia, K. Inoue, Y. Du, S.J. Baker, E. Premkumar Reddy, M.B. Greenblatt, B. Zhao, TGFβ reprograms TNF stimulation of macrophages towards a non-canonical pathway driving inflammatory osteoclastogenesis, Nat Commun 13 (2022). https://doi.org/10.1038/s41467-022-31475-1.
[41] P.O. Marchal, P. Kavvadas, A. Abed, C. Kazazian, F. Authier, H. Koseki, S. Hiraoka, J.J. Boffa, C. Martinerie, C.E. Chadjichristos, Reduced NOV/CCN3 expression limits inflammation and interstitial renal fibrosis after obstructive nephropathy in mice, PLoS One 10 (2015). https://doi.org/10.1371/journal.pone.0137876.
[42] V.T. Monsen, H. Attramadal, Structural insights into regulation of CCN protein activities and functions, J Cell Commun Signal 17 (2023) 371–390. https://doi.org/10.1007/s12079-023-00768-5.
[43] G. Sgalla, C. Franciosa, J. Simonetti, L. Richeldi, Pamrevlumab for the treatment of idiopathic pulmonary fibrosis, Expert Opin Investig Drugs 29 (2020) 771–777. https://doi.org/10.1080/13543784.2020.1773790.

Figure legends

Figure 1. Detection of CCN3 in RA synovial tissues. A) Immunohistochemistry examination of knee and wrist synovial tissues stained with CCN3 antibody. Scale bars are 50 μM. B) Expression of CCN3 in the synoviocytes of RA clinical samples analyzed via scRNA sequencing. The left panel shows t-SNE plots for synoviocyte clusters. The right panels represent the expression of CCN3 and the inflammatory marker FAP in the cells. C) Percentages of cells positive for CCN3 and FAP in each cluster. D) Expression of CCN3 in

the synoviocytes of experimental murine RA samples analyzed via scRNA sequencing. The left panel represents t-SNE plots for cell types in the joint. The right panels represent the expression of CCN3 and the inflammatory marker FAP in the cells. E) Percentages of cells positive for CCN3 and FAP in each cell type.

Figure 2. CCN3 stimulation results in the activation of the senescence pathway in synoviocytes in vitro. A) Volcano plot representing the molecular response of hFLSs (n = 3) to stimulation with recombinant CCN3. Red plots represent significantly upregulated genes, and blue plots represent significantly downregulated genes. B) KEGG pathway enrichment analysis of the differentially upregulated genes. C, D) Gene Ontology analysis of the differentially upregulated genes. E) Heatmap illustrating differentially expressed genes involved in the senescence pathway identified via RNA-seq. E) Venn diagram analysis of the genes significantly upregulated in stimulated FLSs and those associated with senescence/aging in tissues. G) Heatmap illustrating differentially expressed genes associated with the aging of tissues identified via RNA-seq. H) Detection of senescence markers via Western blot analysis. The panels on the right represent the quantification of protein expression. I) Senescent FLSs were detected by immunostaining with β-gal. FLSs were stimulated with recombinant CCN3, fixed and stained with an antibody. In the bar charts, the symbols represent individual samples, and the bars represent the means ± SEMs. Significant differences were determined by two-tailed Student's *t* test. * = $P < 0.05$; *** = $P < 0.001$.

Figure 3. CCN3 administration results in the activation of the senescence pathway in joints. A) Experimental procedure for the administration of CCN3 in the knee joint. B) Histological evaluation after administration of CCN3. The left panels are representative images of HE- and pP53 antibody-stained sections. The right panel represents the percentage of pP53 cells in the sections. D) Detection of β-gal-positive cells in synovial tissues. The left panels are representative images of sections stained with a β-gal antibody. The right panel represents the percentage of β-gal-producing cells in the sections. Scale bars, 100 μM. In the bar charts, the symbols represent individual samples, and the bars represent the means ± SEMs. Significant differences were determined by two-tailed Student's *t* test. * = $P < 0.05$.

Figure 4. CCN3 stimulation promotes osteoclastogenesis and senescence in human monocytes in vitro. A) Osteoclast differentiation assay. Human monocytes were stimulated with recombinant MCSF plus either RANKL or CCN3 for 8 days and then subjected to TRAP staining. The left panels are representative images of TRAP-stained cells. The panels on the right represent the number of TRAP-stained cells in each well. B) Actin ring formation in stimulated cells. The cells were fluorescently stained with phalloidin for detection of the actin ring (red) and cell nuclei (blue). Scale bars represent 100 μm. C) Bone resorption area on dentine slices generated from stimulated cells. The right figure shows the bone resorption area on a dentine slice. The right panels present the results of the quantitative analysis. D) Volcano plot representing the molecular response of human monocytes to stimulation with recombinant CCN3 for 8 days. Red plots represent significantly upregulated genes, and blue plots represent significantly downregulated genes. E) KEGG pathway enrichment analysis

of the differentially upregulated genes. F) Heatmap illustrating differentially expressed genes associated with osteoclast differentiation and senescence pathways in stimulated monocytes identified via RNA-seq. G) Gene Ontology analysis of the differentially upregulated genes related to biological processes. H, I) Heatmaps illustrating differentially expressed genes associated with the TGF-β signaling (H) and focal adhesion (I) pathways in stimulated monocytes identified via RNA-seq. J) Transcriptional regulatory network enrichment analysis of the DEGs. K) Detection of senescent macrophages by immunostaining with β-gal. FLSs were stimulated with recombinant CCN3, fixed and stained with a β-gal antibody. The left panels are representative images of β-gal-stained cells. The right panel represents the percentage of stained cells. In the bar charts, the symbols represent individual samples, and the bars represent the means ± SEMs. Significant differences were determined by two-tailed Student's *t* test. * = $P < 0.05$.

Figure 5. CCN3 administration to calvarial bone results in a local increase in the number of osteoclasts and senescent cells. A) Experimental procedure for the administration of CCN3 to calvarial bone. B) Osteolytic lesions triggered by administration of CCN3 to calvarial bone tissues as determined by micro-CT. The left panels are representative images of the micro-CT images. The right panels present the results of the quantitative analysis of the osteolytic area in the calvarial bone tissues of the mice. C) Detection of osteoclasts via TRAP staining. The left panels are representative images of TRAP-stained sections. The right panels present the results of the quantitative analysis of the TRAP-stained areas in the calvarial bone tissues. D) Detection of senescent cells in calvarial

bone tissues. The left panels are representative images of sections stained with pP53 and β-galactosidase antibodies. The panels on the right represent the percentage of stained cells. Scale bars are 100 μM. In the bar charts, the symbols represent individual samples, and the bars represent the means ± SEMs. Significant differences were determined by two-tailed Student's *t* test. * = $P < 0.05$, **** = $P < 0.0001$.

Figure 6. Therapeutic effects of CCN3 blockade in a CAIA model. A) Experimental procedure of the CAIA model and treatment. B) Arthritis clinical scores of the mice over a period of 28 days. C) Histological evaluation of inflammatory scores. The left panels are representative images of HE-stained sections of right hind paws. The right panels show the quantification of the inflammatory area in the joint. D) Detection of β-gal-positive cells in sectioned joints. The left panels are representative images of immunostained sections of the right hind paws. The panels on the right represent the percentage of β-gal-positive cells. E) Detection of TRAP-positive cells in sectioned joints. The left panels are representative images of TRAP-stained sections of right hind paws. The panels on the right represent the percentage of stained area. Scale bars are 100 μM. In the bar charts, the symbols represent individual samples, and the bars represent the means ± SEMs. Significant differences were determined by two-tailed Student's *t* test. * = $P < 0.05$

A

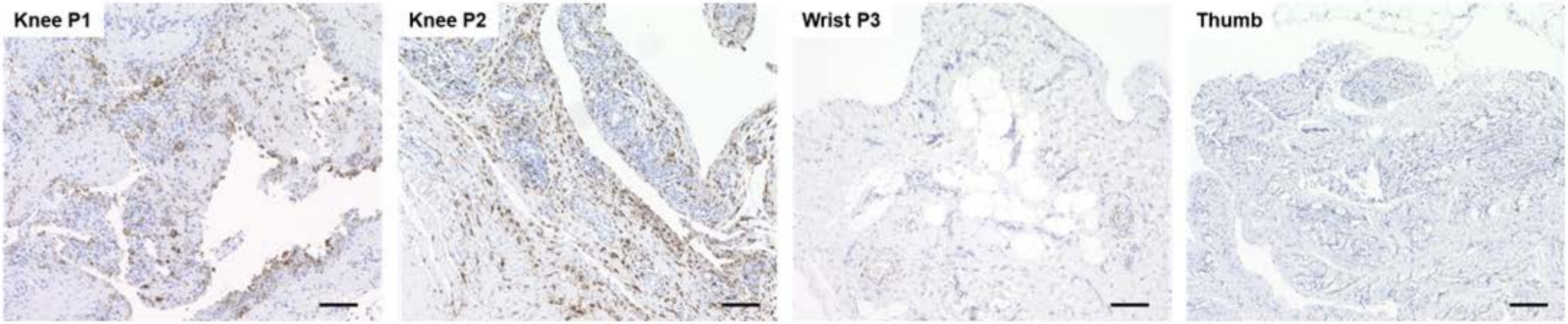
Knee P1
Knee P2
Wrist P3
Thumb

B


Cluster 1
Cluster 2
Cluster 3
Cluster 4
FAP
CCN3
3
0

C

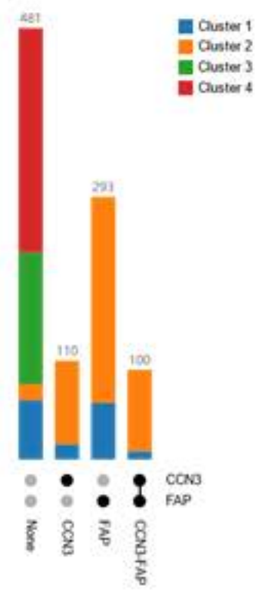
Cluster 1
Cluster 2
Cluster 3
Cluster 4
481
110
293
100
CCN3
FAP
None
CCN3
FAP
CCN3-FAP

D

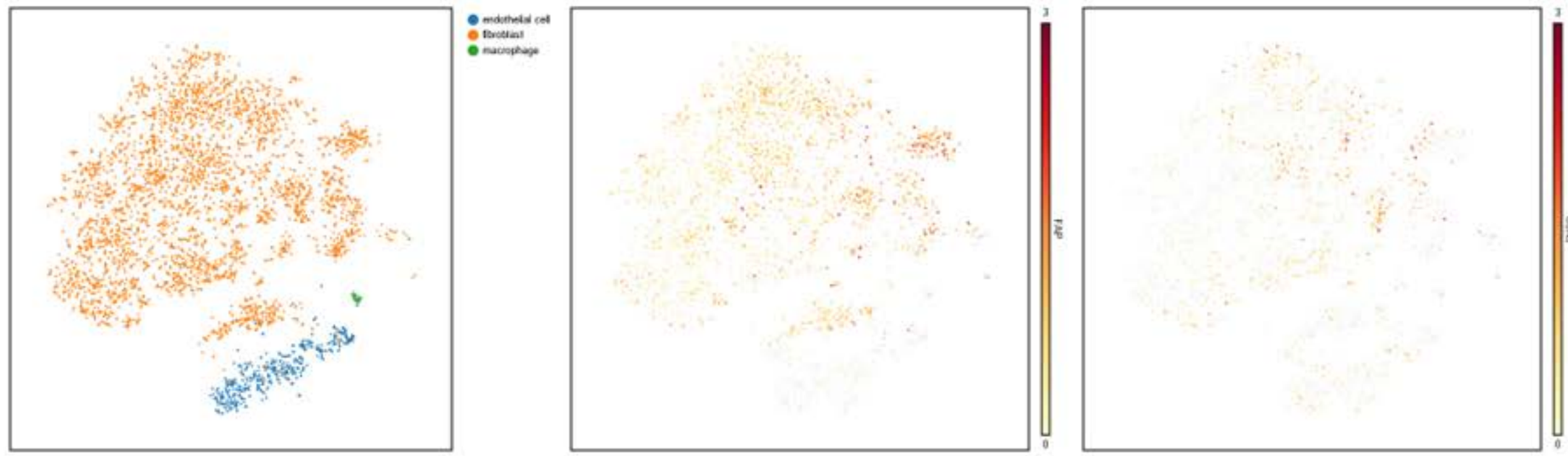
endothelial cell
fibroblast
macrophage
FAP
CCN3
3
0

E

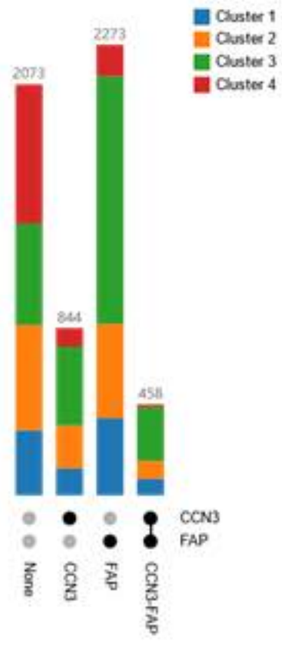
Cluster 1
Cluster 2
Cluster 3
Cluster 4
2073
844
2273
458
CCN3
FAP
None
CCN3
FAP
CCN3-FAP

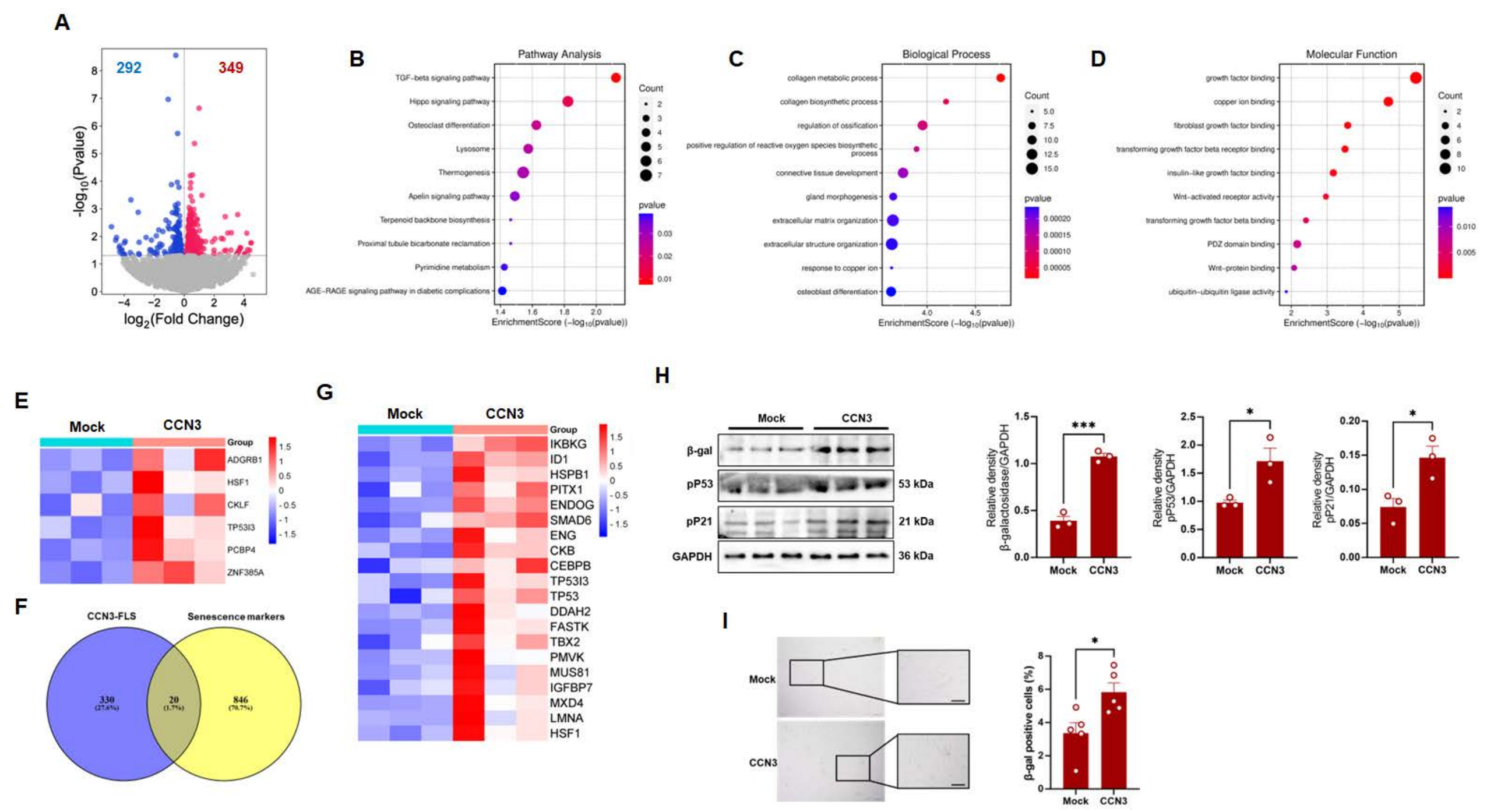
A
292
349
-log10(Pvalue)
log2(Fold Change)
B
Pathway Analysis
TGF-beta signaling pathway
Hippo signaling pathway
Osteoclast differentiation
Lysosome
Thermogenesis
Apelin signaling pathway
Terpenoid backbone biosynthesis
Proximal tubule bicarbonate reclamation
Pyrimidine metabolism
AGE-RAGE signaling pathway in diabetic complications
EnrichmentScore (-log10(pvalue))
Count
pvalue
C
Biological Process
collagen metabolic process
collagen biosynthetic process
regulation of ossification
positive regulation of reactive oxygen species biosynthetic process
connective tissue development
gland morphogenesis
extracellular matrix organization
extracellular structure organization
response to copper ion
osteoblast differentiation
EnrichmentScore (-log10(pvalue))
Count
pvalue
D
Molecular Function
growth factor binding
copper ion binding
fibroblast growth factor binding
transforming growth factor beta receptor binding
insulin-like growth factor binding
Wnt-activated receptor activity
transforming growth factor beta binding
PDZ domain binding
Wnt-protein binding
ubiquitin-ubiquitin ligase activity
EnrichmentScore (-log10(pvalue))
Count
pvalue
E
Mock
CCN3
Group
ADGRB1
HSF1
CKLF
TP53I3
PCBP4
ZNF385A
F
CCN3-FLS
Senescence markers
330
(27.6%)
20
(1.7%)
846
(70.7%)
G
Mock
CCN3
Group
IKBKG
ID1
HSPB1
PITX1
ENDOG
SMAD6
ENG
CKB
CEBPB
TP53I3
TP53
DDAH2
FASTK
TBX2
PMVK
MUS81
IGFBP7
MXD4
LMNA
HSF1
H
Mock
CCN3
β-gal
pP53
pP21
GAPDH
53 kDa
21 kDa
36 kDa
Relative density β-galactosidase/GAPDH
Relative density pP53/GAPDH
Relative density pP21/GAPDH
I
Mock
CCN3
β-gal positive cells (%)

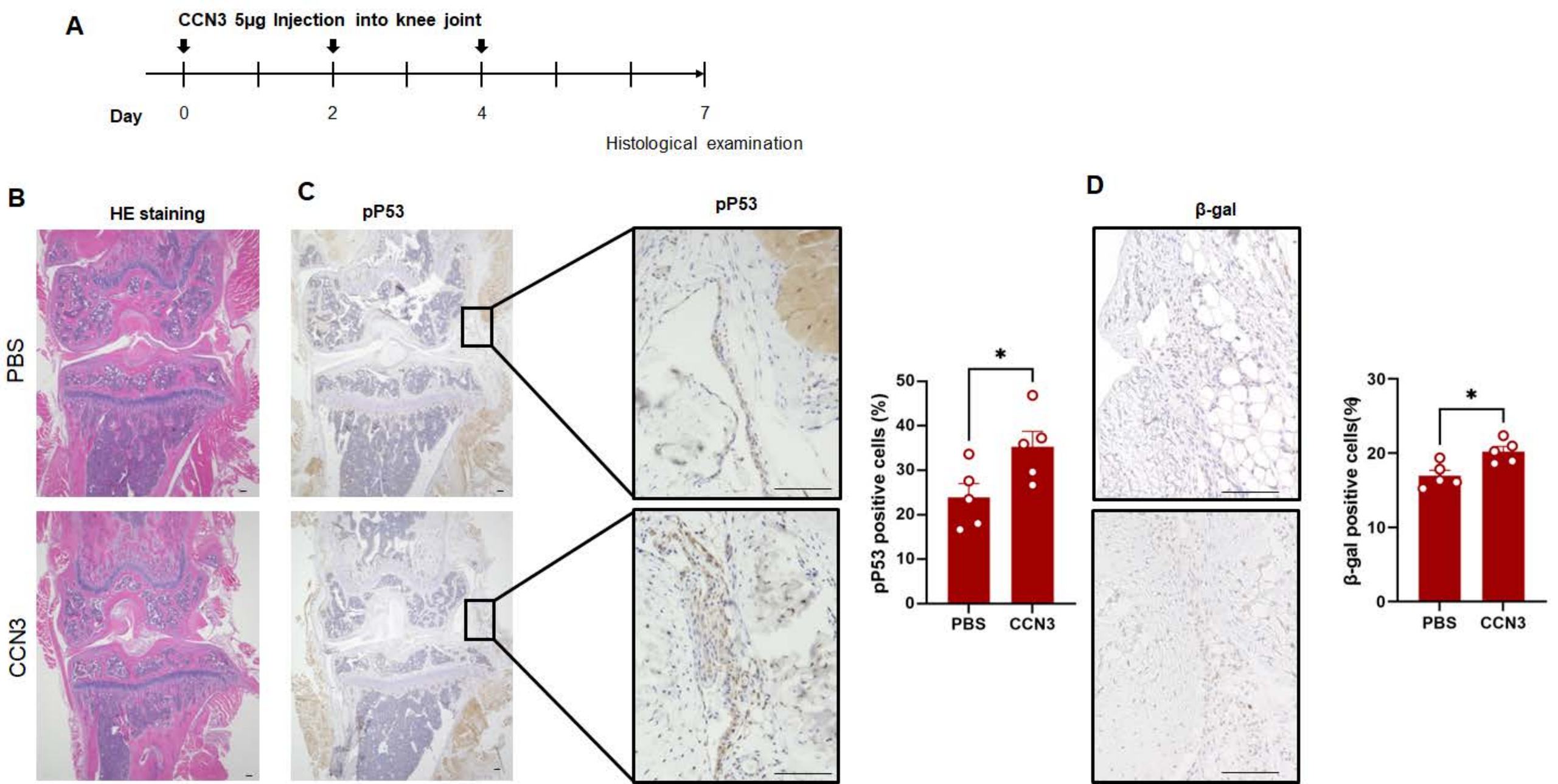
A
CCN3 5μg Injection into knee joint
Day
0
2
4
7
Histological examination
B
HE staining
PBS
CCN3
C
pP53
pP53
D
β-gal
pP53 positive cells (%)
50
40
30
20
10
0
PBS
CCN3
*
β-gal positive cells(%)
30
20
10
0
PBS
CCN3
*

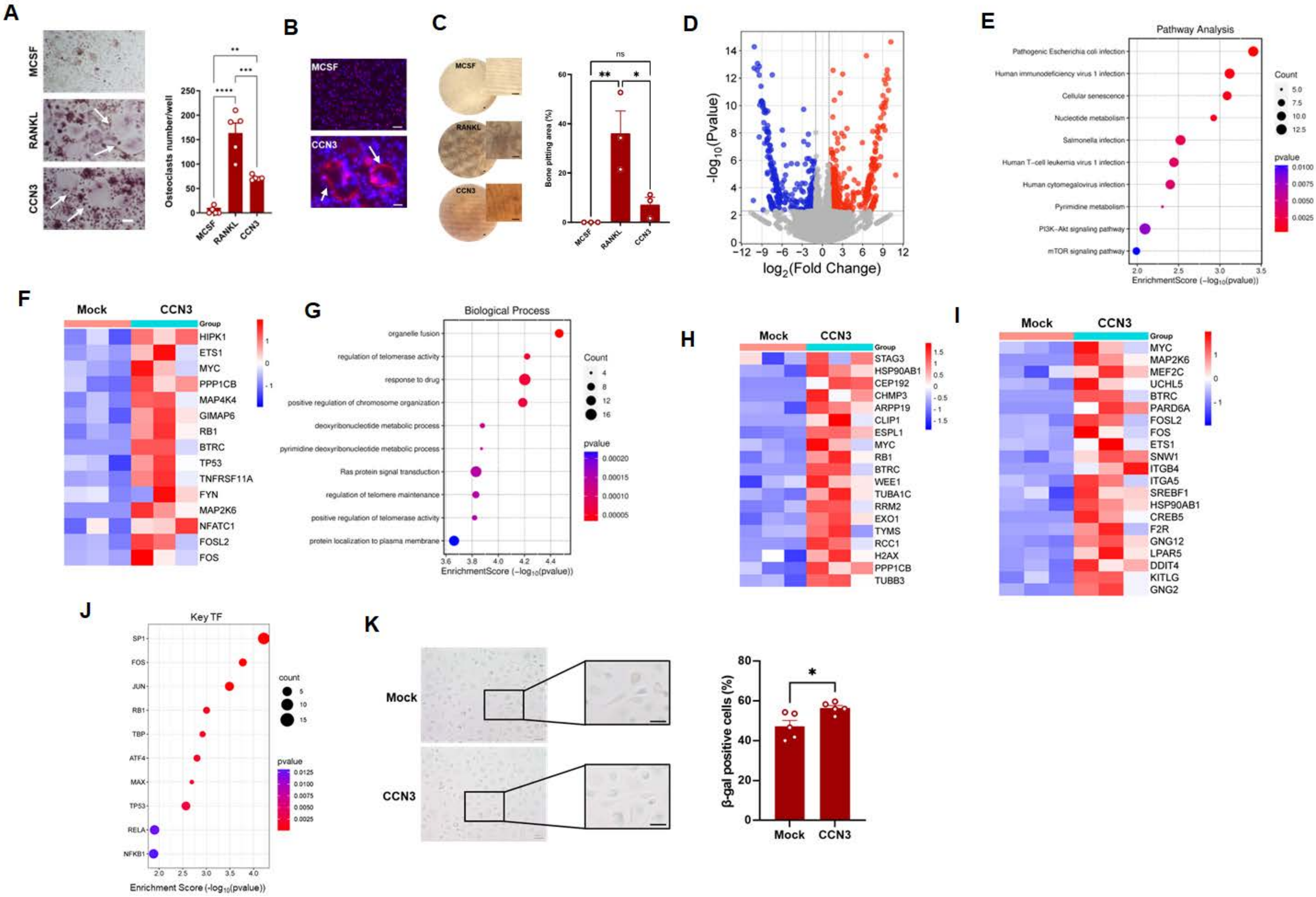
A
MCSF
RANKL
CCN3
Osteoclasts number/well
B
C
Bone pitting area (%)
ns
D
-log10(Pvalue)
log2(Fold Change)
E
Pathway Analysis
Pathogenic Escherichia coli infection
Human immunodeficiency virus 1 infection
Cellular senescence
Nucleotide metabolism
Salmonella infection
Human T-cell leukemia virus 1 infection
Human cytomegalovirus infection
Pyrimidine metabolism
PI3K-Akt signaling pathway
mTOR signaling pathway
Count
pvalue
EnrichmentScore (-log10(pvalue))
F
Mock
CCN3
Group
HIPK1
ETS1
MYC
PPP1CB
MAP4K4
GIMAP6
RB1
BTRC
TP53
TNFRSF11A
FYN
MAP2K6
NFATC1
FOSL2
FOS
G
Biological Process
organelle fusion
regulation of telomerase activity
response to drug
positive regulation of chromosome organization
deoxyribonucleotide metabolic process
pyrimidine deoxyribonucleotide metabolic process
Ras protein signal transduction
regulation of telomere maintenance
positive regulation of telomerase activity
protein localization to plasma membrane
Count
pvalue
EnrichmentScore (-log10(pvalue))
H
Mock
CCN3
Group
STAG3
HSP90AB1
CEP192
CHMP3
ARPP19
CLIP1
ESPL1
MYC
RB1
BTRC
WEE1
TUBA1C
RRM2
EXO1
TYMS
RCC1
H2AX
PPP1CB
TUBB3
I
Mock
CCN3
Group
MYC
MAP2K6
MEF2C
UCHL5
BTRC
PARD6A
FOSL2
FOS
ETS1
SNW1
ITGB4
ITGA5
SREBF1
HSP90AB1
CREB5
F2R
GNG12
LPAR5
DDIT4
KITLG
GNG2
J
Key TF
SP1
FOS
JUN
RB1
TBP
ATF4
MAX
TP53
RELA
NFKB1
count
pvalue
Enrichment Score (-log10(pvalue))
K
Mock
CCN3
β-gal positive cells (%)

A

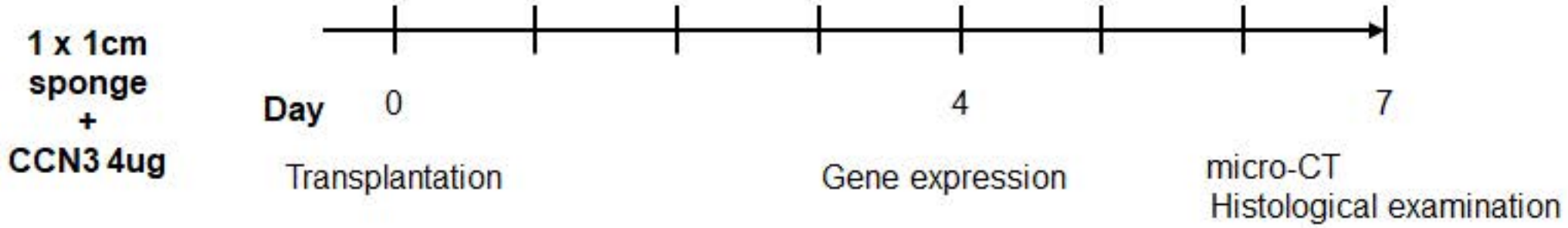
1 x 1cm
sponge
+
CCN3 4ug
Day
0
4
7
Transplantation
Gene expression
micro-CT
Histological examination

B

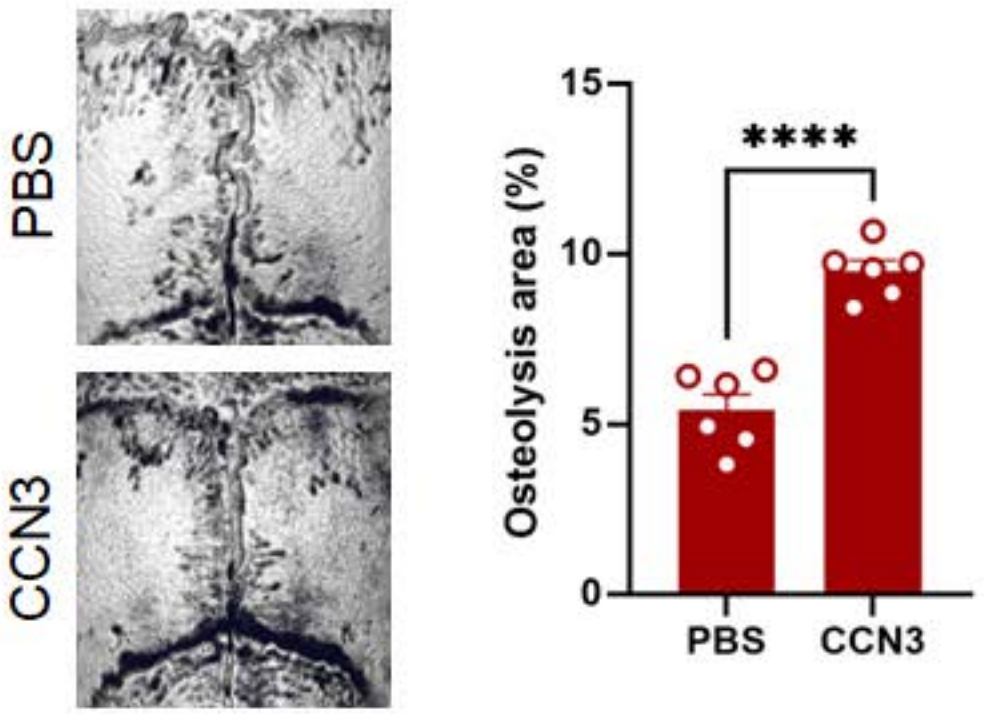
PBS
CCN3
Osteolysis area (%)
15
10
5
0
****
PBS
CCN3

C

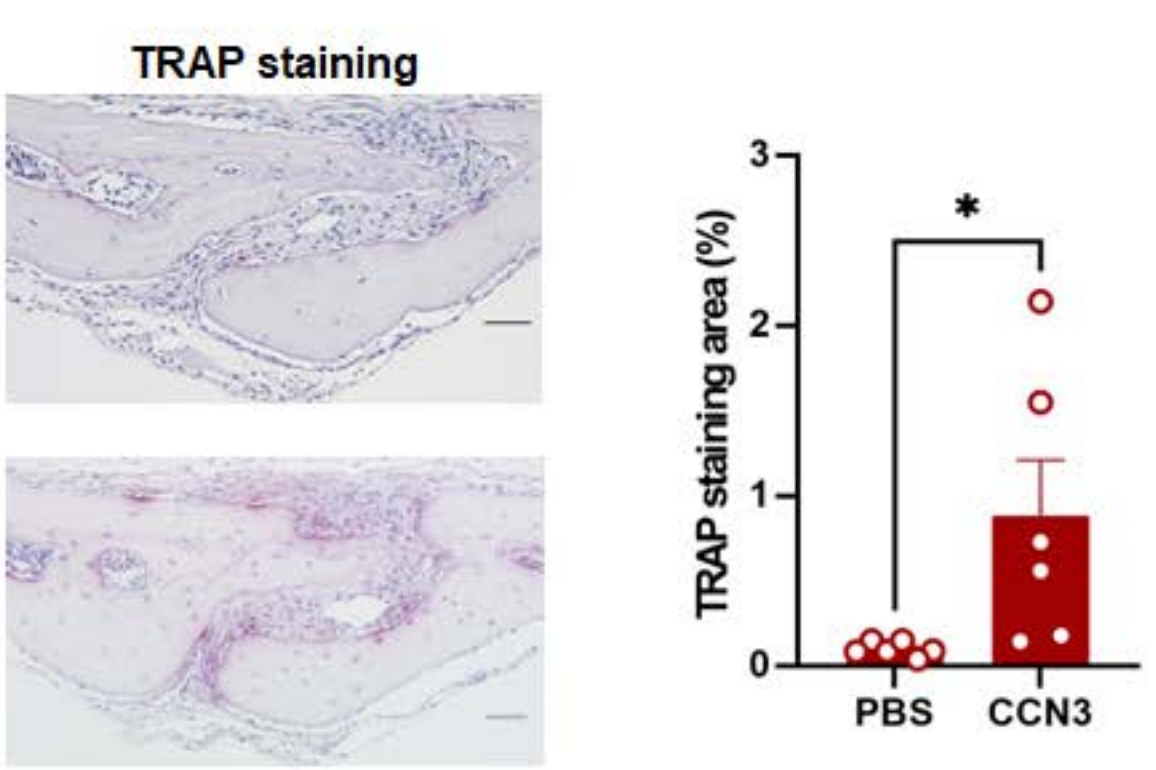
TRAP staining
TRAP staining area (%)
3
2
1
0
*
PBS
CCN3

D

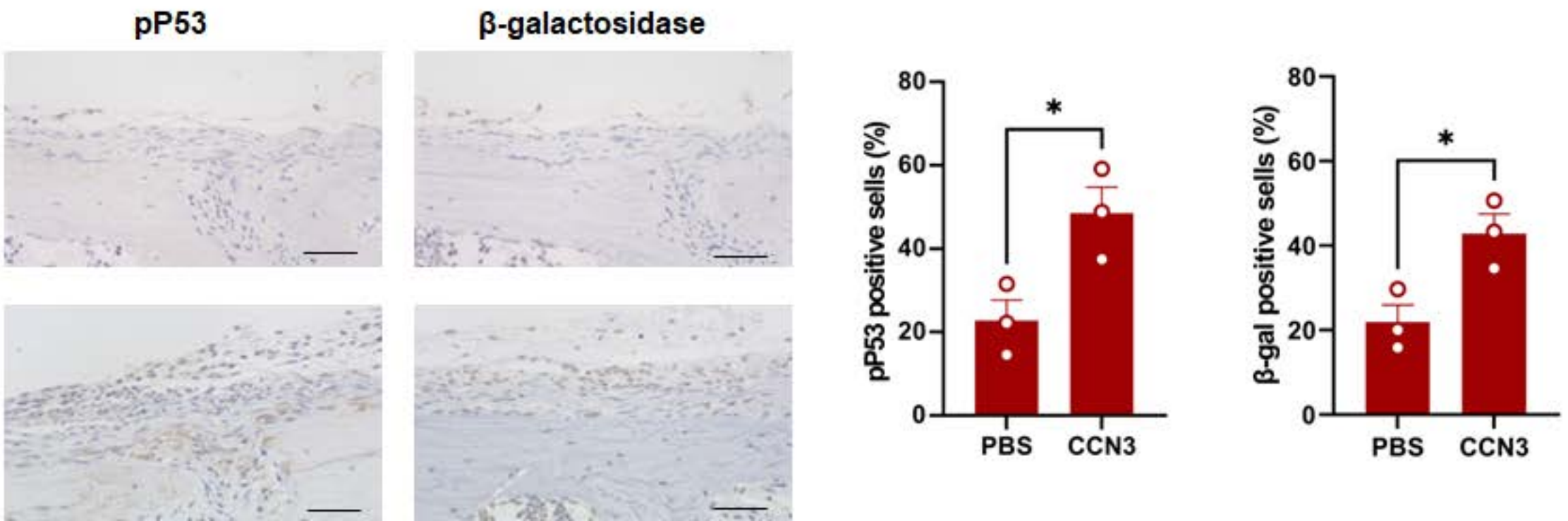
pP53
β-galactosidase
pP53 positive sells (%)
β-gal positive sells (%)
80
60
40
20
0
*
PBS
CCN3

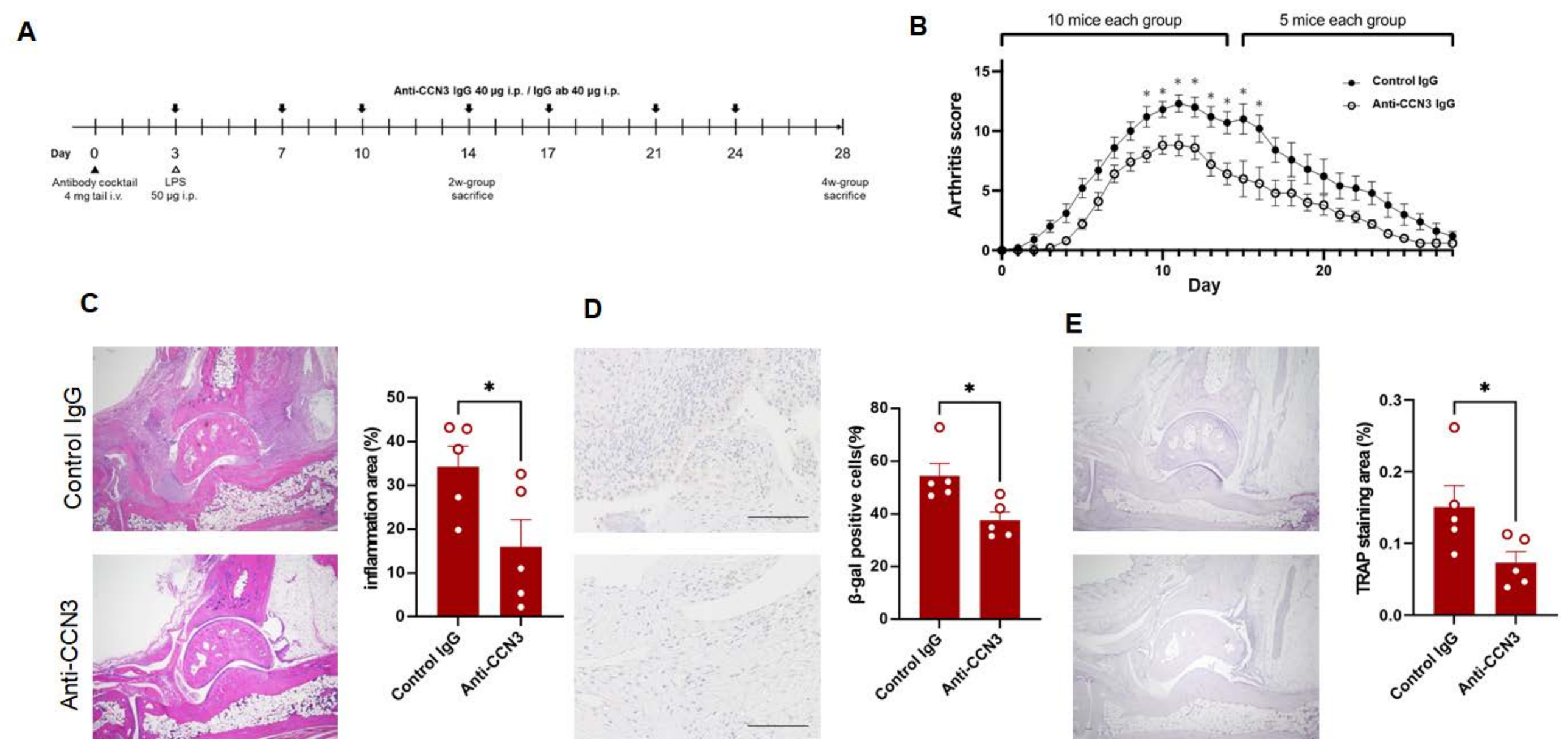
A
Anti-CCN3 IgG 40 μg i.p. / IgG ab 40 μg i.p.
Day 0 3 7 10 14 17 21 24 28
Antibody cocktail 4 mg tail i.v.
LPS 50 μg i.p.
2w-group sacrifice
4w-group sacrifice
B
10 mice each group
5 mice each group
Arthritis score
Day
Control IgG
Anti-CCN3 IgG
C
Control IgG
Anti-CCN3
inflammation area (%)
Control IgG
Anti-CCN3
D
β-gal positive cells(%)
Control IgG
Anti-CCN3
E
TRAP staining area (%)
Control IgG
Anti-CCN3